ACADEMIA BIOLOGY

Research Article
Published: 2024-01-29
https://doi.org/10.20935/AcadBiol6169

The edge of chaos is that where consciousness manifests itself through intermittent dynamics

Valeriy Sbitnev[1,2,*]

Academic Editor(s): Gabriel Gutiérrez-Ospina, Valerio Napolioni

Abstract

Consciousness is a special type of interaction between subjects that is exchanged by lingua quanta (phonemes). A set of lingua quanta composes a thesaurus placed on the edge of chaos. Its library is a memory, modification of which is due to tuning of memristive neural elements scattered in the brain volume. The memristive neural model considers two types of neurons, excitatory and inhibitory, and current leakage at body temperature (T = 310 K). At such temperatures, only heavy ions, such as hydrogen ions (protons), can pass robustly through the water medium of the brain. Robust ion transport involves proton water wires supported by the Grotthuss mechanism. The final aims of the ions are the gap junctions (electric synapses) linking the nearest neurons. Following these observations, a model of excitable nervous tissue was constructed. One-to-one mapping written on the basis of sigmoid curves is capable of reproducing chaotic modes of neural activity, as proved by positive values of the Lyapunov exponent. The edge of chaos is located near the bifurcation boundary dividing chaos and the periodic convulsive activity typical of epileptic discharges. In this region, self-sustained spiral waves occur. Intermittent activity of competing excitatory and inhibitory neurons is observed at the edge of chaos. The intermittent electrical activity of neural tissues is shown by records both from different literature issues and records made by the author and Dr. A. Dudkin on slices of the CA1 field of the hippocampus.

Keywords: *intermittency, Lyapunov exponent, memristor, Grotthuss mechanism, gap junctions, hippocampus*

Citation: Sbitnev V. The edge of chaos is that where consciousness manifests itself through intermittent dynamics. *Academia Biology* 2024;2. https://doi.org/10.20935/AcadBiol6169

1. Introduction

Where how does the brain store information and extract it at the right moment? This question has been worrying scientists for hundreds of years, and there is still no definite answer to it [1–4]. The search for material memory carriers inside the brain did not yield anything intelligible. This problem is getting worse because extensive brain damage does not always lead to violations of brain functions related to human intellectual activity. Such facts bring a significant amount of confusion to the scientific community.

Scientists' opinions on consciousness and its connection with the living brain vary significantly. Some believe that the carrier of consciousness is the material brain. They say that consciousness is engaged in a permanent search for novelty and errors, accompanying new perceptions, to neutralize their influence [5,6]. Others go much further, even to the point of recognizing that consciousness has its roots in the other world [7,8]. John Eccles [9], for example, proposed that the whole world of consciousness, the mental world, is micro-granular, with mental units called psychons, and that in mind–brain interaction, each psychon is linked to its own dendron by quantum laws. In addition to the quantum manifestation of consciousness, many other studies have used different approaches [10–16].

A large volume of scientific publications is devoted to the problem of how the nervous tissues of the brain can organize the preservation of memory traces, quick access to memory, selection of behavior instructions necessary in the current situation. The reciprocal interaction of excitatory and inhibitory neural populations that maintain the balance of excitation and inhibition is of great interest to scientists studying the problem of memory and access to it [17–20]. Obviously, at the beginning, the object of research is formulated—a neural network. It can be defined as a collection of neurons and their interconnections. The most popular network is the Hopfield network [21–23] because of its visual simplicity. This allows us to quickly check certain hypotheses about the associative memory and the functional possibilities of collective computational abilities of the network neurons.

Interesting thoughts were expressed by Charles Sherrington, the great English neurophysiologist of the late 19th century. He spoke figuratively about the brain as follows: It is an enchanted loom where millions of flashing shuttles weave a dissolving pattern, always a meaningful pattern, though never an abiding one; a shifting harmony of subpatterns [24].

[1]Department of Condensed Matter Physics, St. Petersburg B. P. Konstantinov Nuclear Institute, NRC Kurchatov Institute, Gatchina, Leningrad District, 188300, Russia.
[2]Department of Electrical Engineering and Computer Sciences, University of California, Berkeley, CA 94720, USA.
*email: sbitnev_vi@pnpi.nrcki.ru; valery.sbitnev@gmail.com

Surprisingly, this poetic statement about the brain is not so far from the truth. A warm, wet, noisy brain constantly creates random fractal neuronal activity [16] reproducing the consciousness on the edge of chaos [25]. The brain task boils down to the selection of patterns from all these varieties that correspond to the current environment and their tuning and keeping. Nature has found such a selection mechanism. It involves the tuning of memristive elements dispersed throughout the entire neural tissue and the formation of a special thesaurus set. It is this riddle that this article is devoted to.

We proclaim that nature creates different spices by following the most optimal path, often attracting the same proven finds. **Figure 1** shows the memristive Hodgkin–Huxley axon circuit model [26, 27]. Here are three elements: the sodium DC current $V_{Na} - I_{Na}$ through the memristor G_{Na}, the potassium DC current $V_K - I_K$ through the potassium memristor G_K, and the leakage current $V_{G_L} - I_{G_L}$ through the resistor G_L determine the charge on the membrane capacitor C_M.

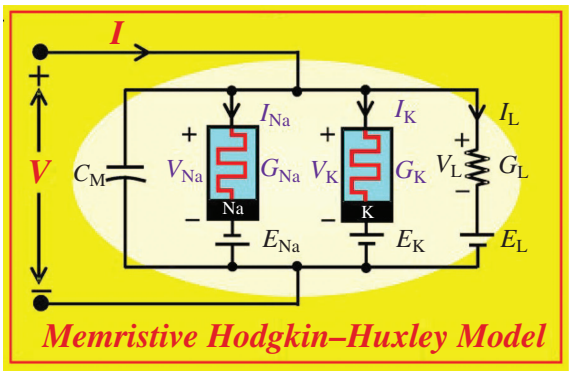

Figure 1 • Memristive Hodgkin–Huxley axon circuit model [26, 27].

A similar circuit diagram occurs for complicated neural tissues containing the interaction of excitatory and inhibitory neurons. In neural tissues containing excitatory and inhibitory neurons, memristive elements determine the conductivities along the neural excitatory and inhibitory links. The memristor conductivities are defined both by the conductivities of the neural membranes and synaptic conductivities (**Figure 2**). Different chemicals underlie this complex conductivity [15, 28–30].

It is impossible to give a complete mathematical description of the nervous tissue shown, for example, in **Figure 2**. Here it is appropriate to quote the statement of Brian J. Ford [31]: "These current concepts (computers will equate to the human brain, V.S.) have acquired an internal self-referential validity, but they concern trite and superficial manifestations of a living system and fail to comprehend its complexity. The self-regulation and capacity for adaptability manifested by each living cell are far beyond the reach of digital computation". From here we can conclude that the mathematical model should confirm the basic principles underlying the functioning of living systems. Examples of such basic ideas can be homeostat, the law of necessary diversity, the principle of self-organization, and the principle of regulatory models formulated by William Ross Ashby [32]. Here we will consider the simplest mathematical model describing the chaotic activity of the excitatory-inhibitory neural system. Lorentz mapping [33,34] underlies this model. The goal is to show that consciousness awakens on the verge of chaos that is adjacent to the border of the onset of epileptic seizures. By the way, the concept of the edge of chaos has

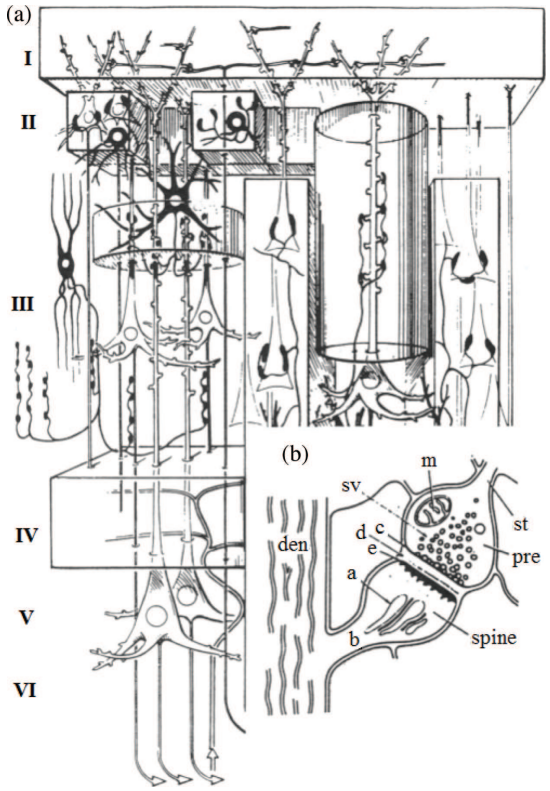

Figure 2 • 3D construct by Szentágothai showing cortical neurons of various types [35]. (a) I, molecular layer; II, external granular layer; III, external pyramidal layer; IV, internal granular layer; V, internal pyramidal layer; VI, polymorphic or multiform layer. (b) Detailed structure of a spine synapse on a dendrite (den). st, axon terminating in synaptic bouton or presynaptic terminal (pre); SV, synaptic vesicles; c, presynaptic vesicular grid; d, synaptic cleft; e, postsynaptic membrane; a, spine apparatus; b, spine stalk; m, mitochondrion. Taken with permission from Ref. [9].

been formulated by Norman Packard [36]. The phrase "the edge of chaos" means metaphorically that some physical, biological, economic, and social systems operate in a region between order and either complete randomness or chaos, where the complexity is maximal.

The article is organized as follows: Section 2 describes a mathematical model that simulates the chaotic activity of the nervous tissue. During the construction of cellular nonlinear mapping, we were guided by the memristive circuit of the Hodgkin–Huxley model, which describes the propagation of the excitation along the nervous axon. Furthermore, we study the chaos region and the bifurcations that lead to chaos. The Lyapunov exponent provides the possibility of defining its region. Section 3 describes chaos, order, and the thesaurus manifold. The latter represents a set of lingua quanta sufficient for the interaction of individuals. This manifold is located on the edge of chaos where the intermittence of fast discharges with slow recovery waves occurs. The brain contains about 70% of water. Therefore, here we study the behavior of protons in this water medium existing at a body temperature about T = 310 K. In Section 4, we consider the detailed organization of the warm, wet, and noisy brain, predominantly near the limbic system. Section 5 is immersed in the consideration of electrical activity in the fields of the hippocampus. The edge of chaos adjoins the onset of convulsive attacks, leading to epilepsy. Note that consciousness that is highly susceptible to subtle external emanations occurs on this edge of chaos. Section 6 gives conclusion remarks

about human consciousness and being escorted by intermittent dynamics.

2. Memristive model of neural tissue

The memristive circuit shown in **Figure 1** for the Hodgkin–Huxley model axon [37], in fact, reflects the balance of currents flowing through sodium, potassium, and the leakage channels. This circuit follows from applying Kirchhoff's laws for the circuits of the electrical network. It is noteworthy that that the same idea of the balance of currents was applied by van Vreeswijk and Sompolinsky [17,18] for describing balanced excitatory and inhibitory activity simulating chaos in neuronal networks. Following to the memristive circuit (**Figure 1**) as a universal circuit for many physical systems, we write the following balanced difference equation:

$$C_{\mathrm{T}}\frac{V(t+\delta t)-V(t)}{\delta t} = \overbrace{G_{\mathrm{E}}V_{\mathrm{E}}S\left(\beta_e\frac{V(t)-V_{\mathrm{E_{th}}}}{V_{\mathrm{tm}}}\right)}^{\text{Excitatory memristor}} - \overbrace{G_{\mathrm{I}}V_{\mathrm{I}}S\left(\beta_i\frac{V(t)-V_{\mathrm{I_{th}}}}{V_{\mathrm{tm}}}\right)}^{\text{Inhibitory memristor}} - \underbrace{G_{\mathrm{l}}V(t)}_{\text{leakage}}. \tag{1}$$

The first curly bracket on the right-hand side embraces the excitatory memristive element. The second curly bracket does the same with the inhibitory memristive element. The third curly bracket embraces the leakage of currents due to imperfect tissues and is also induced by thermal fluctuations. Here all units have dimensions. Namely, C_{T} is the tissue capacitor, V is voltage, G_{E}, G_{I}, and G_{l} are the conductance of the excitatory neural system, inhibitory one, and leakage, respectively. The time step, δt, is about 10 ms. It is approximately equal to the duration of the spikes. Also $V_{\mathrm{E_{th}}}$ and $V_{\mathrm{I_{th}}}$ are thresholds of the excitatory and inhibitory neural cells (**Figure 2**) and V_{tm} is an average level of thermal fluctuations expressed in voltages.

A temperature of approximately 310 K corresponds roughly to the temperature of the human body. The thermal energy of the neural tissue $k_{\mathrm{B}}T$ is about 4.26×10^{-21} J. Expressed in electron volts, the value is as follows:

$$V_{\mathrm{tm}} = k_{\mathrm{B}}T/e \approx 27\,\mathrm{mV}, \tag{2}$$

where e is the electron charge. The thermal fluctuations expressed through the electric currents were observed to lie within the range of the currents through the membranes [38].

Furthermore, we use the value V_{tm} for reducing all voltage variables to dimensionless variables. Preliminarily we divide Eq. (1) by V_{tm}. All these reductions of the variables involved in Eq. (1) are presented in **Table 1**:

Table 1 • Mapping dimensional variables to dimensionless ones

$\frac{V(t)}{V_{\mathrm{tm}}}$	$\frac{V_{\mathrm{E_{th}}}}{V_{\mathrm{tm}}}$	$\frac{V_{\mathrm{I_{th}}}}{V_{\mathrm{tm}}}$	$G_{\mathrm{E}}\frac{\delta t}{C_{\mathrm{T}}}\frac{V_{\mathrm{E}}}{V_{\mathrm{tm}}}$	$G_{\mathrm{I}}\frac{\delta t}{C_{\mathrm{T}}}\frac{V_{\mathrm{I}}}{V_{\mathrm{tm}}}$	$G_{\mathrm{l}}\frac{\delta t}{C_{\mathrm{T}}}$
⇓	⇓	⇓	↓	↓	↓
x_t	v^e_{th}	v^i_{th}	$g_e v^e = q_e$	$g_i v^i = q_i$	ε

Except for the first dimensionless parameter, x_t, which is the driven variable, all the other five parameters in this table are control parameters. Here v^e_{th} and v^i_{th} are dimensionless excitatory and inhibitory thresholds, g_e and g_i are rough dimensionless conductance of the excitatory and inhibitory neural conglomerates (see **Figure 2a**). To further reduce the number of control parameters, we use the dimensionless excitatory and inhibitory conductances $q_e = g_e v^e$ and $q_i = g_i v^i$. Also ε is dimensionless leakage conductance. There are two more control dimensionless parameters—β_e and β_i regulating slopes of the nonlinear functions $S(x)$ (for arguments x of these functions, see in Eq. (1)). Because of these seven control parameters—v^e_{th}, v^i_{th}, q_e, q_i, β_e, β_i, and ε—one can choose the mode of the memristive model at one's discretion. Note that both nonlinear functions $S(x)$ are sigmoid functions. For simplicity, consider the following representation, as in [21]:

$$S(x) = \frac{1}{1+e^{-x}} = \frac{1}{2}\left(1+\tanh\left(\frac{x}{2}\right)\right). \tag{3}$$

2.1. Subtle tuning of the memristive functions

In contrast to the rough conductance of g_e and g_i defined by the states of the cellular membranes and the intercellular washing fluid, the parameters β_e and β_i determine states of the synaptic conductance (see **Figure 2b**). These two parameters allow for subtle tuning of the excitatory and inhibitory conductances. This is due to the enormous amount of synaptic vesicles contained in synapses and the type of mediators stored within these vesicles. Mediators (neurotransmitters) are biologically active chemicals through which an electrochemical impulse is transmitted from a nerve cell through the synaptic space between neurons (**Figure 2b**). Traditionally, neurotransmitters belong to three groups: amino acids, peptides, and monoamines (including catecholamines). Examples: (a) Aspartic acid (asparaginate) is an excitatory neurotransmitter in the neurons of the cerebral cortex; (b) Gamma-aminobutyric acid (GABA, $C_4H_9NO_2$) is the most important inhibitory neurotransmitter in the central nervous system of humans and mammals. In particular, we will deal with electrical synapses called gap junctions.

Now we can rewrite Eq. (1) reduced to the dimensionless parameters:

$$x_{t+1} = (1-\varepsilon)x_t + q_e S(\beta_e(x_t - v^e_{\mathrm{th}})) - q_i S(\beta_i(x_t - v^i_{\mathrm{th}})). \tag{4}$$

Here, we normalize the increment δt to the unit and, consequently, $t = 0,1,2,\ldots$. This system includes seven control parameters— ε, $q_e = g_e v^e$, $q_i = g_i v^i$, v^e_{th}, v^i_{th}, β_e, β_i. This set of control parameters is redundant. One can simplify this system if we note that GABA is a very powerful neurotransmitter. Its avalanche-like release inhibits numerous excitatory neurons that it affects. In the first approximation, it can significantly simplify the inhibitory effect by substituting the inhibitory sigmoid function with the Heaviside function $\theta(x_t - v^i_{\mathrm{th}})$ equal to zero at $x_t < v_i$ and equal to the unit otherwise. The equation is as follows:

$$x_{t+1} = (1-\varepsilon)x_t + q_e S(\beta_e(x_t - v^e_{\mathrm{th}})) - q_i \theta(x_t - v^i_{\mathrm{th}}). \tag{5}$$

Walter J. Freeman dealing with the sigmoid functions [39, 40] has coupled the thresholds, v^ν_{th}, with the neuron strengths, q_ν ($\nu = e, i$), according to the following rules [33,41]:

$$v^\nu_{\mathrm{th}} = \ln(\exp\{1-q_\nu\} - (1-q_\nu)), \quad \nu = e, i. \tag{6}$$

Due to this coupling, only four control parameters are left—ε, q_e, q_i, and β_e. A characteristic view of the mapping (eq. 5)

in the case of the mode of chaotic oscillations is shown in **Figure 3**. The chaotic oscillations are realized within an area enclosed by the red square. Outside this area, there are only transient regimes.

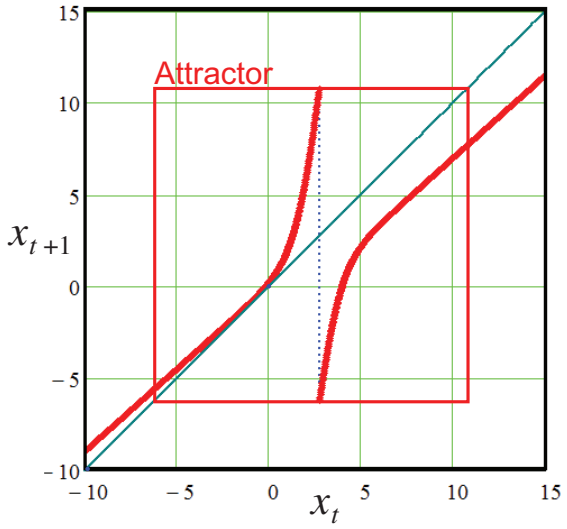

Figure 3 • The mapping (eq. 5) drawn at $\varepsilon = 0.1$, $\beta_e = 0.8$, $q_e = 15$, $q_i = 17$. From Eq. (6) it follows that $v^e_{\text{th}} \approx 2.639$ and $v^i_{\text{th}} \approx 2.773$. The attractor of this mapping lies in the area enclosed by the red square.

Biomolecules such as dopamine $C_8H_{11}NO_2$, serotonin $C_{10}H_{12}N_2O$, adrenalin $C_9H_{13}NO_3$, noradrenaline $C_8H_{11}NO_3$, etc. act as neurotransmitters in nerve cells and play an important role in amplifying and balancing signals in the brain. They provide tuning of neural memristors that support and modify memory traces. In the case of the above difference system (eq. 5), the subtle tuning is achieved by a small variation of the control parameter β_e.

Examples of waveforms reproduced by the mapping (eq. 5) are shown in **Figure 4** for different choosing the control parameter β_e and fixed other parameters.

One can see that at $\beta_e < 0.1$ the oscillations are ordered like a sawtooth with fixed frequencies. While at $\beta_e > 1.322$, the mapping tends to a fixed point somewhere in the vicinity of zero lying on the diagonal. In the interval between the points $\beta_e > 0.1$ and $\beta_e < 1.322$, the oscillations have a pronounced chaotic character. Please note that in the area $\beta > 1$ the duty cycle between bursts begins to grow. Compare the two last waveforms for $\beta = 1.2$ and $\beta = 1.322$. In the last case, the time interval we must stretch up to 4×10^3 units.

This growth of the duty cycle between the bursts with an increase in the control parameter β_e points to the existence of the bifurcation point after which bursts disappear. For more detail analysis of the bifurcations in the mapping under consideration, we calculate the Lyapunov exponent as a function of the control parameter β_e at fixed the other parameters:

$$\lambda = \frac{1}{T}\sum_{t=1}^{T} \ln\left|\frac{dx_{t+1}}{dx_t}\right|_{T\to\infty}. \qquad (7)$$

The results of calculations are shown in **Figure 5**. One can see that there are two bifurcation points, β_e^1 and β_e^2, outside which the Lyapunov exponent is negative. Only between these points, the Lyapunov exponent is positive. This is a region where chaos is in

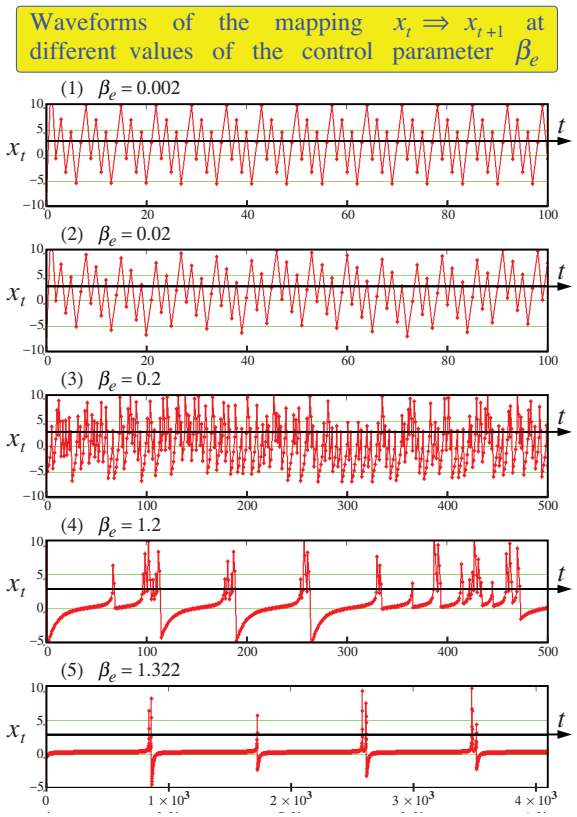

Figure 4 • Waveforms reproducing by the mapping (eq. 5). The control parameters are $\varepsilon = 0.1$, $q_e = 15$, $q_i = 17$. While $v^e_{\text{th}} \approx 2.639$ and $v^i_{\text{th}} \approx 2.773$ are calculated by Eq. (6).

force. Comparison of the Lyapunov exponent shown in **Figure 5** with the data given in the article [25] gives a reason to believe that the edge of chaos is localized from the left of the bifurcation point β_e^2 by adjoining it.

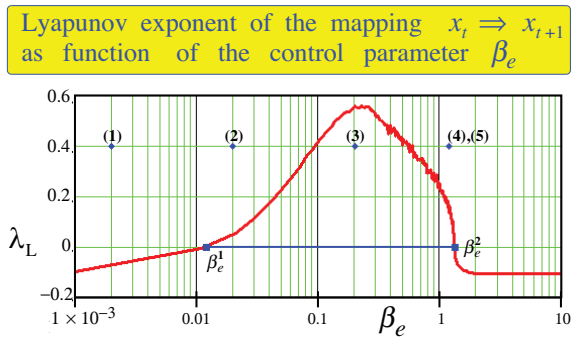

Figure 5 • Lyapunov exponent of the mapping (eq. 5) calculated at the control parameters $\varepsilon = 0.1$, $q_e = 15$, $q_i = 17$, and $v^e_{\text{th}} \approx 2.639$, $v^i_{\text{th}} \approx 2.773$. as follows from Eq. (6). Here $\beta_e^{1,2}$ are bifurcation points. Values (1), (2), (3), (4), and (5) are those at which the waveforms shown in the previous figure are registered.

To complete the picture, **Figure 6** shows the dependence of the Lyapunov exponent on the variation of the control parameters β_e and β_i in the ranges from 0.001 to 2. The edge of chaos is seen to adjoin the bifurcation boundary of β_e^2 from the left side and stretches along it as β_i goes forward further up to infinity. The most impressive pattern of the edge of chaos is observed in the vicinity of the origin of the coordinates. Here, a complicated fractal-like interweaving of the edge of chaos with the region of existence of attractors occurs. This region requires further investigation.

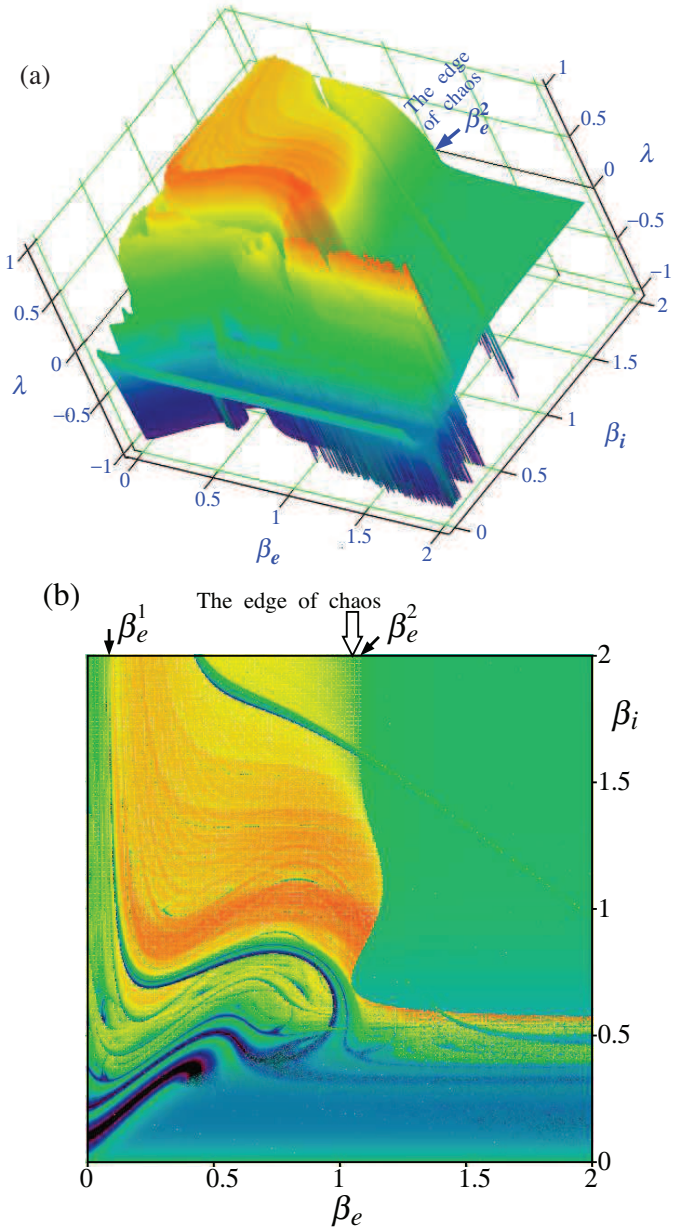

Figure 6 • Lyapunov exponent λ versus the control parameters β_e and β_i computed for the mapping (eq. 4): (a) 3D plot showing the complex relief of the Lyapunov exponent near the origin of the β_e and β_i parameters; (b) bar chart showing the Lyapunov exponent relief, a top view. The minimal and maximal values of the Lyapunov exponent are $\min\lambda = -10.849$ (dark blue) and $\max\lambda = 0.892$ (orange). The remaining control parameters are $\varepsilon = 0.1$, $q_e = 30$, $q_i = 35$, $v_{\text{th}}^e = 3.8$, $v_{\text{th}}^i = 4.6$.

2.1.1. Chaos region

The chaos region extends from $\beta_e^1 \approx 0.0105$ to $\beta_e^2 \approx 1.323$. At these two bifurcation points, different scenarios of transition to chaos occur. In the first case, $\beta_e^1 \approx 0.0105$, the seven-point cycle loses stability; see the upper two waveforms at $\beta_e = 0.002$ and $\beta_e = 0.02$ in **Figure 4**. All points of the seven-periodic waveform in the first record fall at the same places, forming 7 peaks, each having a height of $1/7 \approx 0.143$. The sum of all these peaks is 1. For the second bifurcation point, $\beta_e^2 \approx 1.323$, in this case, the bifurcation proceeds from chaos to a fixed point. The density distribution is represented by a single peak with a height of 1. Histograms demonstrating the density distributions for the seven-periodic cycle at $\beta_e < \beta_e^1$ and for the stable point at $\beta_e > \beta_e^2$ are shown in **Figure 7**.

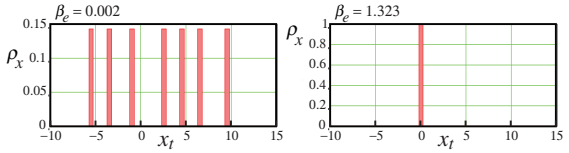

Figure 7 • Histograms of the density distribution ρ_x of the mapping $x_t \Rightarrow x_{t+1}$ for two limiting cases: the seven periodic cycle at $\beta_e = 0.002$ and the stable point at $\beta_e = 1.323$.

Since between $\beta_e^1 \approx 0.0105$ and $\beta_e^2 \approx 1.322$ the Lyapunov exponent demonstrates positive values (**Figure 5**) then a chaotic activity occurs within this interval. The density distribution ρ_x within the observed interval is blurry. A complicated transition occurs between the two stable regimes. The histograms shown in **Figure 8** demonstrate density distributions evaluated between these bifurcation points.

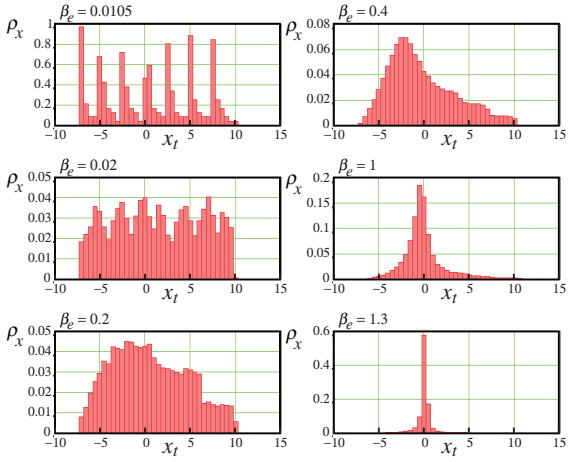

Figure 8 • Histograms of the density distribution ρ_x of the mapping $x_t \Rightarrow x_{t+1}$ chosen from the chaos region $\beta_e \in (0.0105, 1.322)$.

One can see that at β_e changing between 0.01 and 0.2 reformation of the density distribution from the seven peaks induced by the seven-periodic cycle to fluctuations about a single peak with blurred edges occurs, as shown in **Figure 8** for $\beta_e = 0.4$ and $\beta = 1$.

It makes sense to consider chaotic wanderings about a single peak near the second bifurcation point. In this case, the analysis of the mechanisms of selecting different lingua quanta is not difficult. With this aim in mind, let us study Boltzmann entropy and its derivatives of the dynamical system at temperature variations ranging from small values (the ordered states) to high (the chaos states).

3. Chaos, order, and the thesaurus manifold

Temperature of a human body is about T = 310 K. At such a temperature, the thermal noise of the human brain is high enough. At these conditions, there are problems in the selection of lingua quanta against this noise. This selection should provide a guarantee of exchange by lingua quanta with an interlocutor. The problem is to estimate where and under what conditions of noise pollution the optimal sampling of these quanta is possible. In this regard, let us turn to quantum mechanics dealing with processes on the nanolevel. First we write down the wave function in the

polar form:

$$\psi(\vec{r},t) = \sqrt{\rho(\vec{r},t)}\exp\{-iS(\vec{r},t)/\hbar\}. \quad (8)$$

Our proposition is that the lingua quanta are rooted in the action function $S(\vec{r},t)$ (here $\hbar$ is the reduced Planck constant, and $S(\vec{r},t)$ divided by $\hbar$ is a wave phase that quantizes language quanta). While the term $\rho(\vec{r},t)$ determines a density distribution of the lingua quanta per the unit volume of the neuron tissue per the unit of time. We define the quantum entropy as follows [42]:

$$S_Q = -\frac{1}{2}\ln(\rho). \quad (9)$$

It is similar to the Boltzmann entropy $S_B = k_B \ln(N)$, where $N = \rho\Delta V$ is the number of particles occupying a tissue volume ΔV under consideration.

Let now define the number τ that is a control parameter of the entropy of S, varying from zero to some maximum value. It can be, for example, the temperature. When the temperature tends to zero, the entropy turns to zero. In this case, there are no lingua quanta that carry the diversity D. On the other hand, when the temperature reaches high values, there is an excessive variety of different symbols. It leads to noise blurring of the message due to mixing symbol sequences. For that reason, there is a loss of information as the noise increases [43].

There is an optimal range of entropy variations when the message is transferred almost without loss. This range lies in an area where the entropy undergoes significant changes when varying the control parameter τ. Within this range, phonemes demonstrate a diversity of the sound forms that are sufficient to convey meaning. There are no excess sounds that make it difficult to perceive. We name this range the thesaurus manifold (**Figure 9**). This range is where optimal symbols for communications (like phonemes are the minimum semantic units of a language [44]) can be assigned. By definition, a thesaurus or synonym dictionary is a reference work for finding synonyms and sometimes antonyms of words. All these thesauri are in a range where the entropy undergoes significant variations, as shown conditionally in this figure. In our case, the thesaurus manifold is imagined as a customizable memory containing all possible lingua quanta sufficient for communication. Meijer et al. [14, 45–47] have given description of a Musical Master Code based on a generalized musical (GM)-scale of discrete EMF frequencies providing a general communication in Universe.

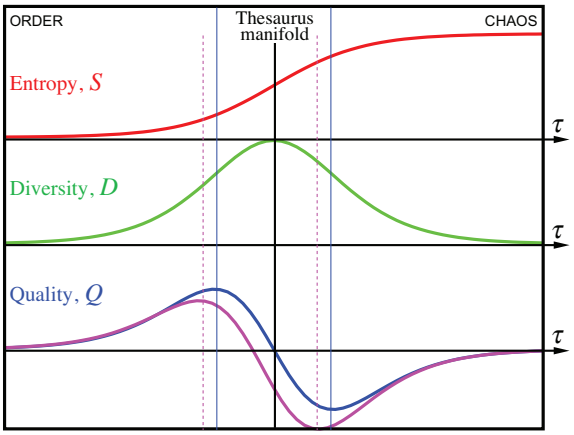

Figure 9 • Entropy S (red). Diversity D (green). Quality Q (blue comes from Eq. (11), magenta from Eq.(12)). On the left, there is a strict order, on the right there is chaos. In the middle, there is a transition from order to chaos. This is where the thesaurus manifold can be located.

If the entropy, $S = -\ln(\sqrt{\rho})$, as a function of τ varies as a sigmoid function shown in **Figure 9** then the diversity, D, calculated by the formula

$$D(\tau) = \frac{dS(\tau)}{d\tau} = -\frac{1}{2\rho}\frac{d\rho}{d\tau} \quad (10)$$

looks like a bell. Let us now calculate the second derivative from S by τ. We will get

$$Q(\tau) = \frac{d^2S(\tau)}{d\tau^2} = \frac{\left(\frac{d\rho}{d\tau}\right)^2}{2\rho^2} - \frac{\frac{d^2\rho}{d\tau^2}}{2\rho}. \quad (11)$$

This curve is shown in **Figure 9** in blue. It characterizes the quality of the thesaurus manifold by extracting it using the negative slope of its derivative. Thin blue vertical lines in this figure allocate the thesaurus manifold. Most effective phonemes for communications are within this interval.

Note that the magenta curve shifted to the left has the following mathematical representation:

$$Q(\tau) = \frac{\left(\frac{d\rho}{d\tau}\right)^2}{4\rho^2} - \frac{\frac{d^2\rho}{d\tau^2}}{2\rho}. \quad (12)$$

Differences between these two curves are in the denominators of the first term. The first blue curve has in the denominator the number 2. While the second magenta curve has in the same place the number 4. Observe that this curve can represent the quantum potential if the control parameter, τ, will relate to the space coordinate $\vec{r}$. In this case, the above equation, accurate to the factor $\hbar^2/2m$, will be as follows [16, 48]:

$$Q(\vec{r}) = \frac{\hbar^2}{2m}\left(\frac{(\nabla\rho)^2}{4\rho^2} - \frac{\nabla^2\rho}{2\rho}\right) = \frac{\hbar^2}{8m}\left(\frac{\nabla\rho}{\rho}\right)^2 - \frac{\hbar^2}{4m}\frac{\nabla^2\rho}{\rho}. \quad (13)$$

The quantum potential is due to the action of Fick's law in a medium where random wanderings of virtual particles take place. It suggests that the quantum lingua memory is distributed over space filled by particles being in equilibrium at a certain temperature of the medium. At this point, it is appropriate to cite the thoughts of David Bohm concerning the connection of consciousness with quantum mechanics. After formulating a causal interpretation of quantum theory [49, 50], David Bohm went far from usual ideas in understanding a connection of quantum mechanics with the mind and the consciousness [51, 52]. A special role here belongs to the quantum potential that distinguishes quantum mechanics from classical ones. Here's what he writes about it in his article [51]:

> Since the quantum potential can be thought of as information whose activity is to guide the "dance" of electrons, there is a fundamental similarity between the quantum behavior of a system of electrons and the behavior of the mind.

Further [51]:

> It is thus implied that in some sense a rudimentary quality like the mind is present even at the level of elementary particle physics and that as we move to more subtle levels, this mental-like quality becomes stronger and more developed. Each species and level of intelligence can have relative autonomy and stability.

This rudimentary quality like the mind can be supported on the border dividing the order and disorder states. In the scientific literature, they say about such a border as the edge of chaos [27,36]. This metaphor means that some physical, biological, economic, and communication systems function in the realm between order and total randomness or chaos, where complexity is maximal. Physical observations say that the maximal complexity occurs near the phase transition points dividing different physical phases [53], either in the vicinity of the bifurcation points of dynamical systems [54,55]. The simplest toy model is a logistic mapping where the edge of chaos is defined by the Lyapunov exponent at crossing it of zero value [34].

Turning to the difference mapping (eq. 5) describing the excitability of the nervous tissue, it can be noted that the thesaurus manifold is adjacent to the second bifurcation point β_e^2 (**Figure 5**). Near this point (the range between 0.2 and β_e^2 in this figure), the activity of the nervous system is characterized by long phases of intermittency of rapid chaotic bursts and slow recovery waves. Characteristic frequencies of the brain are 2–70 Hz. Note that the bifurcation point β_e^2 adjoins the onset of an epileptiform activity. It is accompanied by emergence of the sharp-wave ripple (SW ripple) complexes. Such complexes (**Figure 10**) have been observed in the hippocampus at provocation of epileptiform activity [56]. There is every reason to believe that the appearance of high-frequency ripples in the hippocampus is caused by the hyper-conductivity of gap junctions [28].

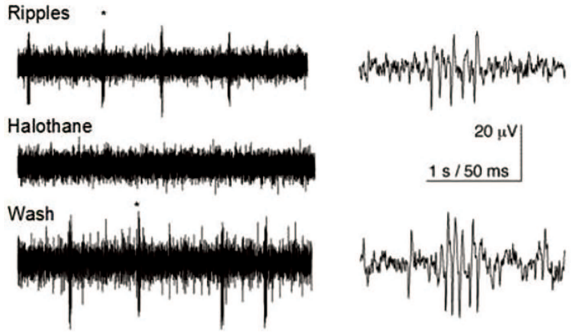

Figure 10 • SW ripples [56] are shown from the left in top. By application of the anesthetic drug halothane, the high-frequency ripple oscillations are abolished. After this drug is washed, SW ripples reappear. Asterisks (*) on the left records indicate the ripples corresponding to the right traces. The timescale 1 s/50 ms means that 1 s relates to the left records and 50 ms deals with the right traces.

As [56] have noted, the mechanisms responsible for ripple generation shown in **Figure 10** are not fully understood; however, there is a suggestion that gap junction proteins play a crucial role.

3.1. Quantum proton transport through water channels. Wet wires and gap junctions

Note that the brain contains about 70–80% of water. For that reason, one can guess that the memory may be distributed over water clusters. For this hypothesis, there are clinical observations of a patient whose brain fluid was found instead of a developed brain [57]. The clusters are permanent fluctuating structures of water fragments at the temperature T about 310 K. It is the human body temperature. At this temperature, electrical fluctuations of the chemical molecules are about 27 mV, which is commensurate with electrical processes on membranes of nerve cells [9,38]. Since all these processes go in a water environment, the first reaction subjected to such electrical fluctuations can be separation of a proton from a water molecule [58].

A free proton has a little lifetime in the water. Evaluations show that the proton mobility in water is about $\delta\tau \approx 2 \times 10^{-13}$ s [59]. It is of interest to evaluate the following value [16]:

$$b = k_B T \delta\tau \approx 8.556 \times 10^{-34} \text{ J} \cdot \text{s}. \tag{14}$$

This value is evaluated at the body temperature $T = 310$ K. Surprisingly, this value is almost identical with the Planck constant $h = 6.626 \times 10^{-34}$ J · s. And that is not all. One more parameter relates to the inertial mass of the hydrogen ion in the water computed as the ratio of thermal energy to the square of the sound speed

$$m_s = k_B T / c_s^2 \approx 1.88 \times 10^{-27} \text{ kg}. \tag{15}$$

It is almost the proton mass $m_p = 1.67 \times 10^{-27}$ kg. For evaluation, we apply the rate $c_s \approx 1500$ m/s at which hydrogen ions move in a salty aqueous solution. In the liquid medium, the sound speed c_s plays a role analogous to the speed of light in the vacuum [60], where the Einstein formula is $E = mc^2$.

Let us evaluate the length of hopping of the hydrogen ion in water per its lifetime $\delta\tau = 2 \times 10^{-13}$ s. We get $\delta r = c_s \delta\tau = 0.3$ nm. It is the nearest position of the hydrogens in the water staying in the fourth phase (**Figure 11a**). One can see that the fourth phase looks like hexagonal packing of hydrogen and oxygen ions by 2D layers. Such hetero structures occur in water at a special temperature, the triple point temperature $T = 273.16$ K. It is simultaneous coexistence of solid, liquid, and gaseous phases of water [58]. The body temperature, however, is about $T = 310$ K. At such a temperature, the hexagonal packing of hydrogen and oxygen ions is destroyed. Note, however, intracellular and extracellular waters are located under special conditions. These waters contain different kinds of biomolecules, providing them corridors of uninterrupted transport to their destinations. This means that

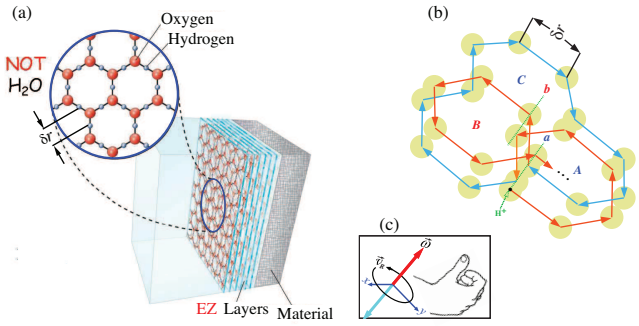

Figure 11 • Fourth phase of water – the exclusion phase [58, 61]: (a) hexagonal packing of hydrogen and oxygen atoms forming the exclusion zone (EZ), with permission of G. Pollack; (b) conditional hopping of the hydrogen ion H^+ performing an intricate dance along the hexagonal packing; (c) hopping of the hydrogen ion according to the right-hand rule induces a magnetic field directed along the vorticity $\vec{\omega}$. This hopping corresponds to moving along red arrows about the centers A and B, shown in figure (b).

water must sometimes go into an exclusion state, which pushes out biomolecules in the right direction. Obviously, these exclusion states are short-lived. However, this fluctuating state is sufficient to ensure the hydrogen ion hopping along this exclusion zone, as shown in **Figure 11b**. As seen there are possible hopping clockwise and counterclockwise. They are drawn in this figure by red and cyan colors, respectively.

Hopping about centers A, B, and C along closed paths induces the vorticity $\vec{\omega}$ oriented either up (for clockwise hopping) or down (for counterclockwise hopping). In **Figure 11c**, these vortices are colored in red and cyan, respectively. The magnetic field induced by a single point electric charge q moving at a speed v_R about a closed path is described by the following formula:

$$\vec{B}(\vec{r}) = \frac{\mu_0 \cdot q}{4\pi} \cdot \frac{[\vec{v}_R \times \vec{r}]}{r^3} \approx 2.67 \times 10^{-4} \text{ T}. \quad (16)$$

Here for the aim of evaluation we take the speed $v_r = c_s = 1500$ m/s and the distance from the central point is $\delta r = 0.3$ nm. For comparison, the electric field at the same input parameters is

$$\mathbf{E}(\vec{r}) = \frac{q}{4\pi\varepsilon_0\varepsilon_r} \cdot \frac{\vec{r}}{r^3} \approx 1.6 \times 10^{10} \frac{\text{V}}{\text{m}} = 16 \frac{\text{V}}{\text{nm}}. \quad (17)$$

Here $\varepsilon_0 = 1/(\mu_0 c^2) \approx 8.854 \times 10^{-12}$ F/m is the vacuum permittivity and $\mu_0 = 4\pi 10^{-7}$ H/m is the magnetic permeability constant. The dimensionless parameter $\varepsilon_r = 81$ represents the relative permittivity of water. It shows how many times the interaction force of two electric charges in a particular medium is less than in a vacuum. The latter has $\varepsilon_r = 1$. From these estimates, it can be seen that the brain is a diamagnetic medium with high electrical conductivity.

Let us choose a distance from the hydrogen ion on 10^5 times more than 0.3 nm. Let it be $r \approx 25$ μm = 2.5×10^{-5} m. This roughly corresponds to the size of the granular neuron cells receiving signals from mossy fibers (see **Figure 2a**, layers I and II). The granular cells are able to combine information from different mossy fibers and create new patterns of activity. Evaluations show that the electric field at this distance falls only up to 28 mV/m, which is almost the same as the thermal noise in the brain. While the magnetic field at the same distance falls up to 3.8×10^{-14} Tesla. Its influence is very weak.

From the above evaluations, it follows that the granular cells are capable of perceiving the hydrogen ions when they are hopping on vacancies in the water clusters, induced by the Grotthuss shuttling mechanism [62, 63]. As a result of this mechanism, the migrating protons "create" nanotubes leading to formation of their own self-sustained water "wires" in hydrophobic spaces [64, 65] (**Figure 12**). The flows of migrating protons along water "wires" represent robust channels of information transfers. An ordered set of such channels providing a flow of many protons enhances the reliability of information transmission.

Due to such channels like the self-sustained water "wires", the warm, wet, and noisy brain may support communication with the subtle superfluid quantum ether. Two crucial parameters make communication possible. The thermal parameter for the hydrogen ion, which is given by Eq. (14), is the first parameter that is close to the Planck constant. The second parameter is the inertial mass of the hydrogen ions in water (eq. 15), which is near the mass of the proton. These conformities bridge the gap between hydrogen ion fluctuations in water and proton fluctuations in vacuum. The

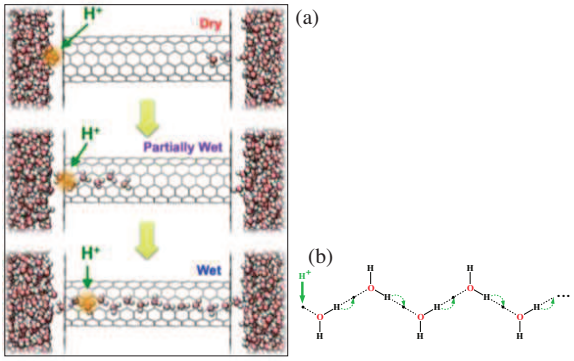

Figure 12 • Grotthuss shuttling transport of an excess proton charge defect along a wet wire: (a) forming a wet wire by the proton induced wetting process (Dry→Partially Wet→Wet) [65] along with the motion of the excess proton along the bulk tube from the left to the right. Water molecules are drawn by the red big sphere (oxygen) with two small gray satellite-spheres (hydrogens); (b) mechanism for proton conduction [66]: a proton enters the chain on the left side and then as a result of the series of proton hops indicated by the arrows, a proton exits the chain on the right.

latter provides a connection with the superfluid quantum medium represented by the Bose-Einstein condensate of coupled proton-antiproton pairs.

It suggests that there may be a connection between brain activity and the ether, and possibly even the dark matter and the dark energy. In this regard, the most intriguing substance, according to the teachings of Vedantic Hinduism, is Akasha [67]. It means the essence and foundation of all things in the material world.

In particular, Eccles in his book "How the Self Controls Its Brain" [7] presupposes the existence of an eternal, unchanging spiritual entity, an absolute, that is aware of its own existence which acts on the brain through the mental units embedded in the brain. Eccles and Beck published the article entitled "Quantum aspects of brain activity and the role of consciousness" [38] where they tried to demonstrate such a communication with the absolute. It is interesting to note that in this article they dealt with the proton as a quantum unit of transferring information. In their approach, the Schrodinger-like equation is capable of describing subtle brain activity at a nanometer level [1, 2, 10, 16, 38, 68].

The nanowire set increasing the transmission conductivity of protons gives a possibility, in the first approximation, to consider the proton bunch as a coherent wave travelling along the formed nanowire channel. By applying the Feynman path integral technique [69–71], we find the amplitude of the transition probability of passing protons along the nanowire channel. Targets of the protons migrating along the nanowire channels are gap junctions (electric synapses with two-way conduction in contrast to one-way conducting chemical synapses, **Figure 1b**). The gap junctions are grouped in discrete regions of the plasma membranes of the contiguous cells. Electronic micrographs of the gap junction sheets disclose that they are tightly packed into a regular hexagonal matrix (**Figure 13**).

The center-to-center spacing between gaps, *d*, can be different for different gap junctions ranging from 6–7 nm, 8–9 nm, up to 20 nm [72]. The gaps can be either open or closed. It is regulated by special proteins that are connexin proteins, and also pannexin proteins. Six such proteins envelop the gap and act like the camera shutter. The gap is closed or opened depending on the turn

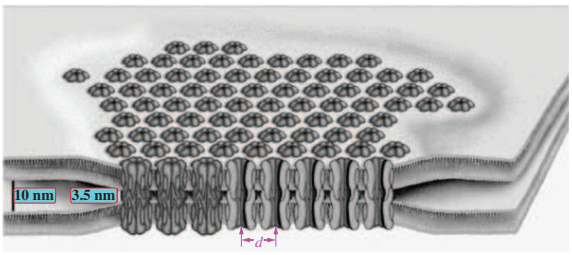

Figure 13 • Schematic representation of gap junctions clustered in a hexagonal array [73]. Gap junctions connect the inner space of two contiguous neurons whose membranes are 10 nm apart from each other. The gaps bring them closer to a distance of 3.5 nm.

of the connexin proteins around the axis of the gap, clockwise or counterclockwise. **Figure 13** shows in the front examples of the closed and opened gaps. Here, the first three gap junctions on the left are shown as closed, while the last five gaps are open. For that reason, the gap junction array represents a memristor channel for ions transferring through the gaps.

The regular hexagonal matrix is seen to be an interference grating containing many slits that tend to remain open from a few seconds to several minutes [73]. Hydrogen ions incident on the grating scatter behind it by the quantum mechanics laws by reproducing in near zones both constructive and destructive interference fringes. The de Broglie wavelength is $\lambda_{dB} = c_s \cdot \delta\tau \approx 0.3$ nm. Let us evaluate the Talbot length $z_T = d^2/\lambda_{dB}$. It is a unit of distance accepted for interference observation [71]. Taking into account the center-to-center spacing of the gap junctions ranging from 6 to 9 nm, we find the Talbot length about 100–300 nm. Such lengths are typical for dendrites of the stellate cells in the molecular layer. Thus, the flow of the hydrogen ions through the gap junctions can modify the internal currents within the stellate neurons, which, in turn, modulate works of the pyramidal neurons.

However, the amount of the gap junctions and their special proteins regulating the capacity of the gaps should be optimal. Otherwise, as was noted earlier this apparatus of gap junctions may lead to either undesirable SW ripple oscillations or can not support proper activity of the nervous tissue. In other words, this apparatus should have a subtle memristive tuning with the neurons which it serves. And all this should be subordinated to the functions of the higher parts of the brain. Here we come to the clarification of these functions.

It is instructive to remind that the mammalian brain consists of about 75% of water. Other 20% are lipids and proteins. Such a fractal mixture of hydrophilic and hydrophobic components makes up what is the carrier of the mind in a warm, wet, noisy brain [16].

There is a transitional bridge in the form of gap junctions, through which fluctuations of hydrogen ions in an aqueous medium are transmitted to fluctuations in the membrane potential of neural fibers washed by extracellular water. Further, these weak membrane oscillations coming from the dendritic fibers are amplified as they pass through these fibers until the axon hillock is reached. The subsequent pattern of excitation development captures adjacent neural nuclei and tissues. Therefore, without a detailed acquaintance with the neuroanatomy of the brain, it will be difficult to understand the holistic picture of the formation of consciousness. Here we will reveal only a small part of this picture, relating to the function of the hippocampus, as a kind of "visual organ" that evaluates impulse flows through this structure.

4. Warm, wet, and noisy brain

As seen the water is a main liquid medium in the brain where all important events occur. Although dendrites and axon terminals of neurons of the brain penetrate through all brain space everywhere densely, there are spaces relatively free from the nervous filaments. These spaces are ventricles of the brain filled by the cerebral liquid. In medical practice, there is a case when a 44-year-old patient with the postnatal hydrocephalus of unknown cause [57] showed by the magnetic resonance imaging (MRI) that his brain has hypertrophied brain ventricles (**Figure 14**). The deficit of the filamentous organization demonstrates massive enlargement of the lateral, third, and fourth ventricles, with a very thin cortical mantle and a posterior fossa cyst. Surprisingly, however, this patient possesses normal social functions and has an intelligence quotient (IQ) of about 75. This example gives an indirect hint at the fact that the cerebral liquid, a slightly brackish water, has a direct relationship to cognitive functions of the brain.

As **Figure 14** shows, only a thin layer adjoining the cranial box represents neural tissue. The rest of the space in the skull is occupied by cerebrospinal liquid washing the dendritic processes. It is that case, when the gap junctions washed by the liquid play a crucial role. For comparison, it is suggested to look at **Figure 15** showing the horizontal incision of the brain going through the lateral ventricles of the brain. One can see that an area occupied by the ventricles is smaller than those shown in **Figure 14**. However the liquid filling these ventricles wash the hippocampus from all sides rather tightly. In fact, the left and right hippocampal arcs are fully immersed in the cerebral liquid. Perhaps, a neighborhood of the hippocampus with such a water basin plays a crucial role for its functions, since we know that the water is a source of free protons arising due to thermal fluctuations.

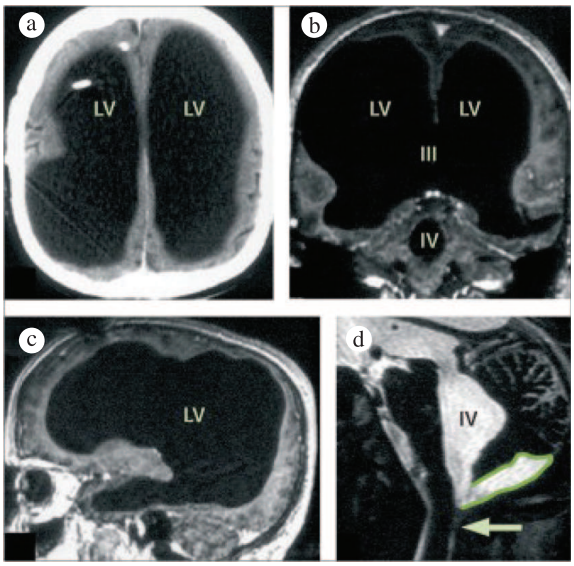

Figure 14 • Massive ventricular enlargement, in a patient with normal social functioning: (a), (b), (c) MRI with gadolinium contrast at different cross-sections; (d) T2-weighted MRI. LV = lateral ventricle. III = third ventricle. IV = fourth ventricle. Arrow points to Magendie foramen. The posterior fossa cyst is outlined in (d). Taken from Ref. [57].

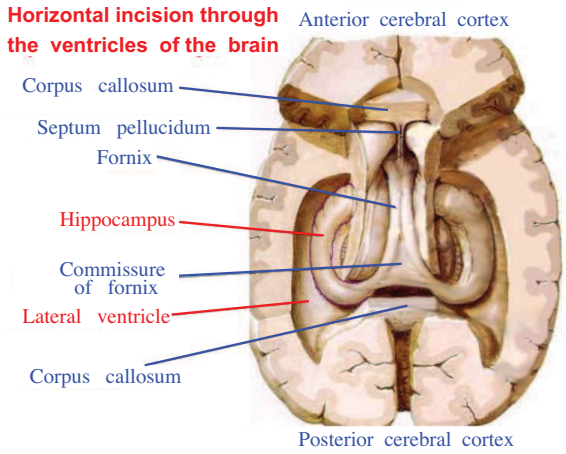

Figure 15 • Horizontal incision through the ventricles of the brain. Taken from presentation on the topic of Brain parts (In Russian) [74].

It makes sense to show the position of the hippocampus in the brain and its place among other important brain tissues (**Figure 16a**). This whole construction covers the nuclei of the thalamus. The thalamus, in turn, has many connections with the amygdala and hippocampus through the mammillothalamic tract, which includes the mammillary bodies and the fornix (**Figure 16b**). The medial surface of the thalamus rests on the third ventricle of the brain, whereas the arches of the hippocampus border with the lateral ventricles. It means that this amazing structure bordering with the cerebral water basins has the ability to receive an influx of free protons arising in the cerebral water due to thermal fluctuations. For that it must have a well-developed, balanced apparatus of gap junctions for the quick transport of thermal protons arising in water to neural cells [28, 75–78].

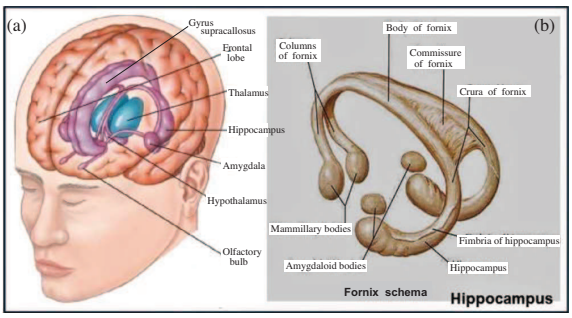

Figure 16 • Neural tissues composing the limbic system [47]: (a) Thalamus (blue) is a sensitive subcortical nucleus, a collector of sensitivity. Main functions [79]: integration of all types of sensitivity (subcortical pain center, where the pain sensation is formed), comparison of information, and evaluation of its biological significance. Hippocampus (colored in violet) is part of the limbic system of the brain (the olfactory brain) and the hippocampal formation. It participates in the mechanisms of emotion formation, memory consolidation (i.e., the transition of short-term memory to long-term memory), and spatial memory necessary for navigation [80, 81]; (b) Fornix scheme looks like an interferometer devise.

5. Specific functions of the hippocampal fields

In the previous section, such important subcortical structures as the thalamus and hippocampus were mentioned. Both structures border on the ventricles of the brain, which brings a bit of mystery to these structures.

Wilder Penfield was convinced that the human brain—including areas of the cortex—is controlled and organized through a group of subcortical centers. These centers are located in the upper brain stem and include the thalamus (**Figure 16a**). Consciousness and self-consciousness depend on the integrating action of this subcortical system, which somehow, as yet unknown, unites the brain into a single functioning organ. These ideas Penfield developed in Sherrington's lectures [82]. By intensely studying people suffering from epilepsy at surgical treatment of this condition, he disclosed that these people have an increased sensitivity to occurring events. At some surgical interventions in the temporal regions of the brain, these people experienced vivid visual or auditory hallucinations (the book "Epilepsy and the Functional Anatomy of the Human Brain" [83] contains detailed descriptions of these remarkable observations on temporal epilepsy).

As discovered by Wilder Penfield, a revolutionary in the understanding of the human brain [84], stimulation of the temporal lobes provokes hallucinations, dreams, strikingly vivid memories, up to out-of-body experiences [85, 86]. It points to a primary function of the temporal lobes as the physical basis for memory [87]. As can be seen in **Figure 16a**, nervous tissues adjacent to the temporal regions are the hippocampal arcs. There is reason to believe that the hippocampus performs a function similar to effectors such as eyes perceiving light, ear snails perceiving sound, or nostrils perceiving smell. The only difference is that the pair of hippocampal arches (**Figure 16b**) located in the temporal lobes of the brain receive the input signals from the entorhinal cortex. And next the hippocampus by the Shaffer collateral sends resulting excitation through the subiculum [88] back to deep IV–VI layers of the entorhinal cortex; see organization of the layers in **Figure 2a**. The most striking manifestation of hippocampal activity is the intermittency of fast discharges and slow recovery waves in the ranges of characteristic frequencies of the brain (alpha, gamma, delta biorhythms). This activity is characteristic of the edge of chaos, where it is possible to implement a variety of electric patterns.

Since the hippocampal structures provide supporting the brain biorhythms, they are sensitive for provoking epileptic seizures [83]. A large amount of work is devoted to a thorough study of the onset and development of these seizures initiated by various methods in the hippocampus [89–96]. In fact, in all records of electrical activity illustrating the onset of convulsive activity, one can see the intermittency of fast bursts with slow waves of recovery. **Figure 17** being taken from [89] shows evolution of the intermittency dynamics at spontaneous seizure recorded in an epileptic patient.

Figure 18a shows the internal organization of the hippocampus depicted in the cross-section of the hippocampal arc. Pathways linking the hippocampus with the entorhinal core through the subiculum are tuned for supporting the standard brain biorhythms. They are alpha, beta, gamma, and delta rhythms. These rhythms play a crucial role in the organization of the functional activity of the hippocampus for recognition and accumulation of new data in the long-lived memory [80]. Observe that this structure works like a comparator [5, 6, 81, 97].

Figure 18a is very remarkable. It was made by Camillo Golgi in 1894, by the method stained with the silver nitrate first proposed

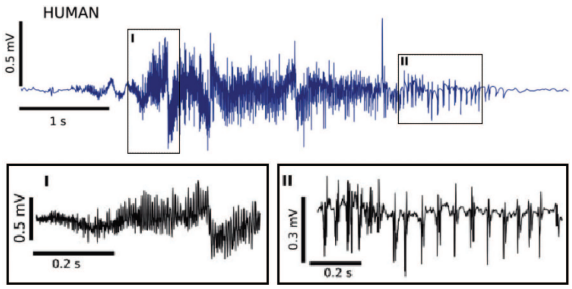

Figure 17 • Spontaneous seizure recorded in an epileptic patient [89] displaying fast discharges, panel I, followed by the occurrence of sharp bursts convoying by wave events shown in panel II.

and used by him. Surprisingly, the organization of the hippocampus is very similar to the retina of the human eye, with well-oriented pyramidal cells. It can hint that the hippocampal pyramidal cells process the input pulse flows in such a manner as the retina does. Note that Nature prefers to use repeatedly once found solutions by slightly modifying their functions. As we know, the retina receiving the light falling on it converts it into chemical energy. Whereas, the hippocampal cells receive the impulse flow from the entorhinal cortex and sort them according to the rhythm, coming from the dentate gyrus (DG). Just as the retina of the eye performs saccades along the object being viewed, the hippocampus does the same when sorting or sampling memory traces. Such a scenario is achieved by the intermittent neural activity that is like the sharp jumps with slow wave relaxations. The comparator described by scientists, Gray [97], Vinogradova [6], Kryukov [81], and Numan [98], for the explanation of the hippocampal functions compares the current state of the perceptual

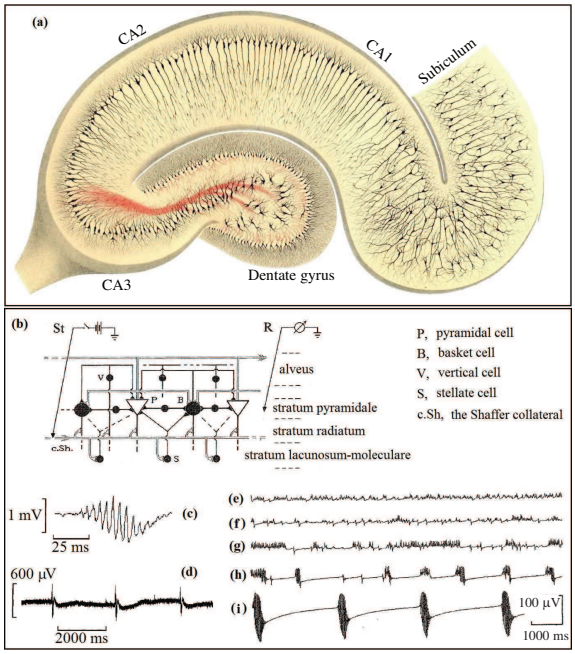

Figure 18 • Hippocampus: (a) stained with the silver nitrate method by Camillo Golgi in 1894 exhibits principal cells of the hippocampus; (b) principal types of neurons, pathways, and synaptic connections in the field CA1 of the hippocampus [41]. St and R point to positions of the stimulating and registering electrodes, respectively. The bursting spontaneous activity in hippocampal slices (c) and (d) induced by the application of picrotoxin. Patterns of such an activity are shown in (e), (f), (g), (h), and (i). They have been simulated by varying the coupling strength (conductance of gap junctions) in the coupled map lattice [33].

world with a predicted state. Here the same mechanism of intermittency is used.

The intermittent oscillations in the circuit of the pyramidal and basket neuronal complexes (**Figure 18b**) represent typical activity of the hippocampal neurons [89–96]. With the aim to observe such intermittent bursts, an experiment was conducted by Dudkin and Sbitnev [42] on a slice of nerve tissue taken from the CA1 field of the rat hippocampus. The results are shown in **Figure 18c,d**. It is instructive to compare these records with SW ripples shown in **Figure 10**. In our case, we applied picrotoxin to induce a sequence of the bursts since it acts as a stimulant and convulsive agent due to its interaction with the inhibitory neurotransmitter GABA.

To verify the intermittent mechanism, we simulated it by 2D couple map lattice. The neighbor cells in this lattice are coupled with each other by a diffusion manner. The diffusion mechanism simulates the coupling by the gap junctions. Results of this simulation are shown in **Figure 18e–i**. One can see as the coupling strength increases the chaotic fluctuations are beginning to acquire more and more pronounced signs of intermittency. At increasing the diffusion coupling, the bursts begin to cluster into bundles between which the relaxation intervals grow (**Figure 18g,h**). A further increase in the strength of coupling leads to the formation of strictly ordered bursts (**Figure 18i**). This mode corresponds to the onset of seizure discharges.

Observations show that the seizure discharges involve in their synchronous activity of all other cellular structures on which these discharges are projected. Also the convulsive focus involves in its activity of all nearest cells due to gap junctions that involve in the generation, synchronization, and maintenance of seizure events [96]. Our model of the hippocampal slice [42] has been based on joining the mappings (eq. 4) into a complete cluster representing a 2D cellular nonlinear network (CNN). The diffusion coupling of the nearest cells [99]

$$\begin{aligned} i_{t,n,m} &= \frac{D}{2}\left(\frac{x_{t,n-1,m}-2x_{t,n,m}+x_{t,n+1,m}}{2}\right. \\ &\left.+\frac{x_{t,n,m-1}-2x_{t,n,m}+x_{t,n,m+1}}{2}\right) \\ &= D\left(\frac{x_{t,n-1,m}+x_{t,n+1,m}+x_{t,n,m-1}+x_{t,n,m+1}}{4}\right. \\ &\left.-x_{t,n,m}\right). \end{aligned} \tag{18}$$

simulates the gap junction where the diffusion coefficient D represents the conductance.

2D CNN consists of 512×512 cells. On the boundary of this network ($n = 0$, $m = 0$, and $n = 513$, $m = 513$), we give the Dirichlet boundary condition:

$$x_{t,n,m} = 0, \quad \forall \begin{cases} n = 0, 1, 2, \cdots, 513; & m = 0, \ m = 513 \\ m = 0, 1, 2, \cdots, 513; & n = 0, \ n = 513 \end{cases}. \tag{19}$$

As was noted, the magnitude of the diffusion coefficient D relating to the conductance of the gap junction determines the ability of cells to engage synchronous activity. The more D, the more synchronous activity is.

Figure 19 shows two panels demonstrating active dynamics of 2D CNN [99] for two different values of D. The left panel shows a

snapshot of the 2D CNN activity at $D = 0.68$, and the right panel for $D = 0.7$. There is a clear difference between these two pictures. In the left image, the chaotic activity of the 2D CNN is more pronounced. Whereas in the right picture, it gives way to the tending to the onset of ordered spiral waves. In both cases, it is clearly seen the intermittence of the bursts, shown in dark purple, alternating with the slow waves of recovering, shown in blue.

By increasing the parameter D, the dynamical patterns become more ordered, demonstrating spiral waves that are robust enough as shown in **Figure 20**. It is of interest to note that spontaneous spiral intercellular calcium waves and annihilation of colliding waves were experimentally observed in dissociated brain cell cultures [100], in hippocampal slice cultures [101], and in rat neocortical slices [102]. They may pose intercellular signaling through the gap junctions. The observations say that spiral-like waves are widespread during both resting and cognitive task solving [103].

Figure 21 shows a robust 3D spiral wave activity, named in the literature as the scroll wave [104–107]. Tang et al. [108] have observed 3D wandering waves predominantly shifting along a helical trajectory registered in cortical neurons caused by the deviation of a single mouse whisker. This scroll wave was induced at modelling 3D cell arrays by the Hodgkin–Huxley memristive system (see **Figure 1**) completed in 2017 by team Leon Chua, Hyongsuk Kim, and Valeriy Sbitnev. In this figure, the tips of all spiral waves rotate about points on a ring placed in the (x, y) plane and lying in about the middle part of the z axis. This ring is a hearth of the spiral convulsive activity.

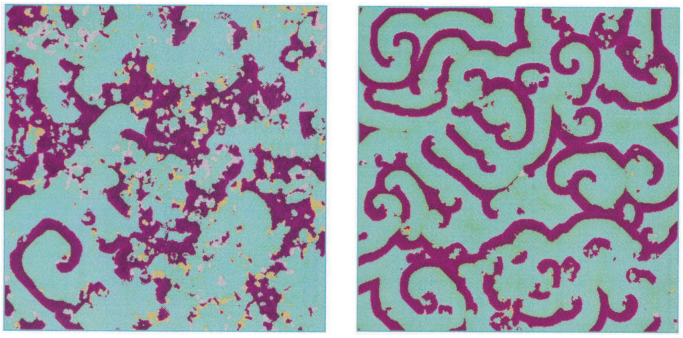

Figure 19 • Spiral-wave turbulence on 2D CNN with the size 512×512 pixels [99], $q_e = 30$, $q_i = 30$. The left panel $D = 0.68$, the right panel $D = 0.7$. The color legend reads $x_{n,m,t} < 0$ is blue. $x_{n,m,t} > 0$ is dark purple, and yellow (wheat) color is for $x_{n,m,t}$ oscillating values about zero.

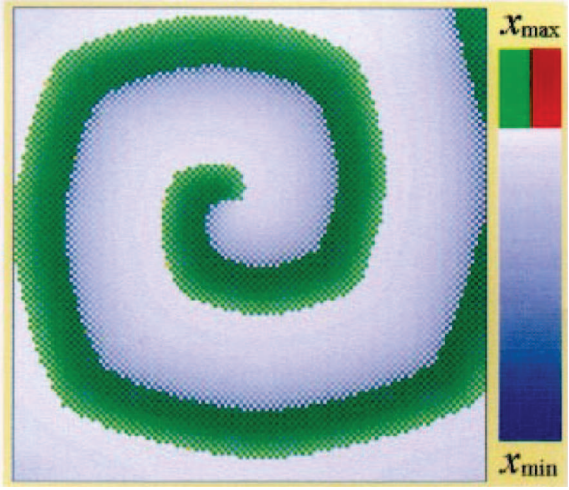

Figure 20 • Checkerboard spiral-wave in 2D Coupled Nonlinear Network, 256×256 pixels [109, 110]. Excitatory and inhibitory control parameters $q_e = 40$, $q_i = 70$. The diffusion coefficient $D = 0.925$.

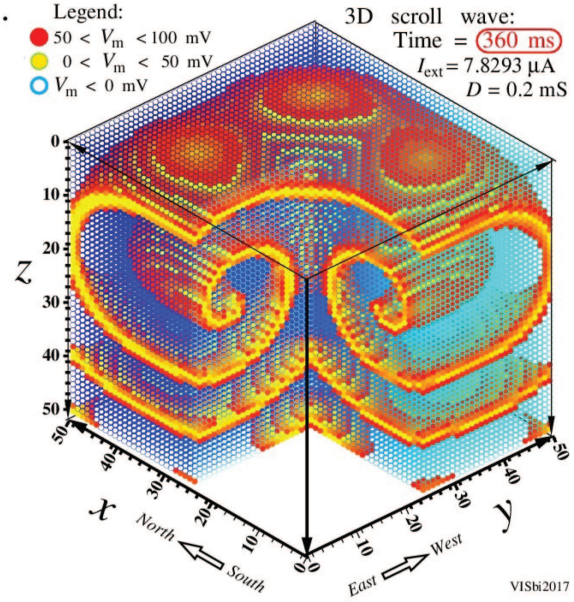

Figure 21 • Scroll wave in 3D array of cells of the memristive Hodgkin–Huxley system. Here the intermittence takes place by the spike bursts (red-yellow crests) accompanied by slow pauses of recoveries (blue areas). This picture was drawn while studying the memristive Hodgkin–Huxley model by the team Leon Chua, Hyongsuk Kim, and Valeriy Sbitnev (Unpublished data). Video of self-sustained scroll wave is accessed on [111].

6. Conclusion

Intermittence is a widespread phenomenon. It manifests in a tunneling quantum effect, as for example, at the Grotthuss shuttling transport in water forming wet water wires. The intermittency is realized as the fast bursts alternating with the slow wave recovery of the electric activity in neural tissues, up to the intermittent effects of consciousness at choosing a goal. So-called saccades along a memory trace storage creating the new combinations from old memory traces and resulting in the emergence of new knowledge. When observing the flow of thoughts at a relaxed state, one can be surprised to find that a thought tracking any idea suddenly jumps to another idea (it is the saccade) that is not connected with the previous one in any way. Then, after a while, the thought can again return to comprehending the previous idea. This is the so-called novelty search effect. A thought can't keep repeating the same image for a long time. The brain needs new sensations. In general, the intermittency is the constant updating of thought patterns.

A natural question arises in which brain structures, where and how does this happen? The efforts of neurophysiologists point to an important function of the limbic system, which includes the thalamus, hippocampus, and other adjacent structures (**Figure 16**). The hippocampus, receiving inputs from the entorhinal cortex (the part of the cerebral cortex located in the temporal lobe and related to the hippocampal formation), processes incoming flows by an intermittent manner on the background of hippocampal biorhythms. Such an intermittent stream is sent back to the entorhinal cortex.

All these functions are made by a wet, warm (temperature is close to $T = 310$ K), and a noisy brain consisting of about 75% water and 20% lipids and proteins (hydrophobic fats). Note that the thermal noise plays a crucial role in updating patterns. Nature has found a way of processing input information in conditions of thermal noise. It is the edge of chaos, which is the area where such intermittent information processing takes place. The processing occurs due to the alternation of the fast bursts with slow waves, recovering states. It gives possibilities for sorting the information flows against the thermal noise background.

One can believe that the human consciousness is a special type of the interaction coupling different individuals to a single organism called society. There are many consciousnesses forming different communities. All consciousnesses are characterized by a common sign—by the intermittence of the fast processes and slow waves of recovery. Due to such an intermittency, the species can exchange information in the presence of a noise background. It leads to formation of self-sustained communities capable of subsequent growth by adapting to new life conditions. The intermittence represents the same "tentacles" (saccades), which open the above freedom for acting. Note that frequencies of the intermittent processes can differ on orders for different consciousnesses.

The Universe is teeming with consciousnesses, which operate on the edge of chaos. The edge of chaos is the area where consciousness is most sensitive to the reception of new ideas. This area adjoins that, where synchronization of the neural activity occurs. These synchronous bursts self-organize in self-sustained spiral waves in a 2D plane or scroll waves in a 3D space. They represent a convulsive activity (the epilepsy attacks).

Acknowledgments

The author thanks Prof. A. Bragin for his discussion relating to the brain functions and the hippocampus. The author also thanks the reviewers of the journal Symmetry for their valuable critical remarks. The author is grateful to the reviewers for their thorough review of the article and valuable comments.

Funding

The author declares no financial support for the research, authorship, or publication of this article.

Author contributions

The author confirms sole responsibility for this work. The author approves of this work and takes responsibility for its integrity.

Conflict of interest

The author declares no conflict of interest.

Data availability statement

Data supporting these findings are available within the article, at https://doi.org/10.20935/AcadBiol6169, or upon request.

Institutional review board statement

Not applicable.

Informed consent statement

Not applicable.

Sample availability

The author declares physical samples were used in the study.

Additional information

Received: 2023-11-21

Accepted: 2023-12-18

Published: 2024-01-29

Academia Biology papers should be cited as *Academia Biology* 2024, ISSN 2837-4010, https://doi.org/10.20935/AcadBiol6169. The journal's official abbreviation is *Acad. Biol.*

Publisher's note

Copyright

References

1. Stapp HP. Attention, intention, and will in quantum physics. J Conscious Stud. 1999;6:8–9.
2. Wolinsky SH. Quantum consciousness. The guide to experiencing quantum psychology. Connecticut: Bramble Books; 1993.
3. Keppler J, Shani I. Cosmopsychism and consciousness research: a fresh view on the causal mechanisms underlying phenomenal states. Front Psychol. 2020;11:371 doi: 10.3389/fpsyg.2020.00371.
4. Di Biase F. Quantum information self-organization and consciousness: a holoinformational model of consciousness. J Nonlocality. 2013;2:1–15.
5. Gray JA. The contents of consciousness: a neuropsychological conjecture. Behav and Brain Sci. 1995;18:659–76. doi: 10.1017/S0140525X00040395.

6. Vinogradova OS. Hippocampus as comparator: role of the two input and two output systems of the hippocampus in selection and registration of information. Hippocampus. 2001;11:578–98. doi: 10.1002/hipo.1073.
7. Eccles JC. How the self controls its brain. Berlin Heidelberg, NY: Springer-Verlag; 1994. doi: 101007/978-3-642-49224-2.
8. Christensen Jr. WJ. God is a Porcupine-Brain, consciousness and spacetime physics. J Mod Phys. 2017;8:1294–318. doi: 10.4236/jmp.2017.88084.
9. Eccles JC. Evolution of consciousness. Proc Natl Acad Sci USA. 1992;89:7320–4. doi: 10.1073/pnas.89.16.7320.
10. Beck F. Quantum mechanics and consciousness. J Conscious Stud. 1994;1:253–5.
11. Hameroff S, Penrose R. Consciousness in the universe: a review of the 'Orch OR' theory. Phys Life Rev. 2014;11:39–78. doi: 10.1016/j.plrev.2013.08.002.
12. Hameroff S. Consciousness, microtubules, & 'Orch OR': a 'space-time Odyssey'. J Conscious Stud. 2014;21:126–53.
13. Tegmark M. The importance of quantum decoherence in brain processes. Phys Rev E. 2000;61:4194–206. doi: 10.1103/PhysRevE.61.4194.
14. Meijer DKF, Jerman I, Melkikh AV, Sbitnev VI. Consciousness in the Universe is tuned by a MusicalMaster code, Part 3: a hydrodynamic superfluid quantum space guides a conformal mental attribute of reality. Quantum Biosyst. 2020;11:72–107.
15. Poznanski RR, Alemdar E, Cacha LA, Sbitnev VI, Brändas EJ. The activity of information in biomolecular systems: a fundamental explanation of holonomic brain theory. J Multiscale Neurosci. 2022;1:109–33. doi: 10.56280/1546792195.
16. Sbitnev VI. Quantum consciousness in warm, wet and noisy brain. Mod Phys Lett B. 2016;30:1650329. doi: 10.1142/So217984916503292.
17. van Vreeswijk C, Sompolinsky H. Chaos in neuronal networks with balanced excitatory and inhibitory activity. Science. 1996;274:1724–6. doi: 10.1126/science.274.5293.1724.
18. van Vreeswijk C, Sompolinsky H. Chaotic balanced state in a model of cortical circuits. Neural Comput. 1998;10:1321–71. doi: 10.1162/089976698300017214.
19. Landau ID, Sompolinsky H. Macroscopic fluctua-tions emerge in balanced networks with incomplete recurrent alignment. Phys Rev Res. 2021;3:023171. doi: 10.1103/PhysRevResearch.3.023171.
20. Stasenko SV, Kazantsev VB. Information encoding in bursting spiking neural network modulated by astrocytes. Entropy. 2023;25:745. doi: 10.3390/e25050745.
21. Hopfield JJ. Neural networks and physical systems with emergent collective computational abilities. PNAS. 1982;79:2554–8. doi: 10.1073/pnas.79.8.2554.
22. Hopfield JJ. Pattern recognition computation using action potential timing for stimulus representation. Nature. 1995;376:33–6. doi: 10.1038/376033a0.
23. Krotov D, Hopfield JJ. Dense associative memory for pattern recognition. In: Lee D, Sugiyama M, Luxburg U, Guyon I, Garnett R, editors. Advances in neural information processing systems. Barcelona, Spain: Curran Associates, Inc.; 2016. Vol. 29.
24. Sherrington C. Man: on his nature. London: The Classics of Medicine Library; 1999. p. 198–207.
25. Toker D, Pappas J, Lendner JD, D'Esposito M. Consciousness is supported by near-critical slow cortical electrodynamics. PNAS. 2022;229:e2024455119. doi: 10.1073/pnas.2024455119.
26. Chua LO, Sbitnev VI, Kim H. Hodgkin-Huxley axon is made of memristors. Int J Bifurcation & Chaos. 2012;22:1230011(48 pp). doi: 10.1142/So218127412300llX.
27. Chua LO, Sbitnev VI, Kim H. Neurons are poised near the edge of chaos. Int J Bifurcation & Chaos. 2012;22:1250098(49 pp). doi: 10.1142/So218127412500988.
28. Traub RD, et al. Gap junctions between interneuron dendrites can enhance synchrony of gamma oscillations in distributed networks. J Neurosci. 2001;21:9478–86. doi: 0270-6474/01/219478-09.
29. Tuszynski J, et al. The archetypal molecular patterns of conscious experience are quantum analogs. J Multiscale Neurosci. 2022;1:41–53. doi: 10.56280/1531676736.
30. Poznanski RR, et al. Spontaneous potentiality as formative cause of thermo-quantum consciousness. J Integr Neurosci. 2018;17:371–85. doi: 10.31083/j.jin.2018.04.0418.
31. Ford BJ. The cell as secret agent - autonomy and intelligence of the living cell: driving force of development. Acad Biol, 2023;10:11. doi: 10.20935/AcadBiol 6132.
32. Ashby WR. An introduction to cybernetics. London: Chapman & Hall; 1956.
33. Sbitnev VI. Noise induced phase transition in a twodimensional coupled map lattice. Complex Syst. 1997; 11:309–21.
34. Ginzburg SL, Sbitnev VI. Spatiotemporal chaos in a 2D coupled map lattice with pinning-like force. Phys D: Nonlinear Phenom. 1999;132:87–99. doi: 10.1016/S0167-2789(99)00030-5.
35. Szentágothai J. The Ferrier lecture, 1977. The neuron network of the cerebral cortex: a functional interpretation. Proc R Soc London B. 1978;201:219–48. doi: 10.1098/rspb.1978.0043.
36. Packard NH. Adaptation toward the edge of chaos. University of Illinois at Urbana-Champaign: Center for Complex Systems Research; 1988.
37. Hodgkin AL, Huxley AF. A quantitative description of membrane current and its application to conduction and excitation in nerve. J Physiol. 1952;117:500–44. doi: 10.1113/jphysiol.1952.sp004764.
38. Beck F, Eccles JC. Quantum aspects of brain activity and the role of consciousness. Proc Natl Acad Sci USA. 1992;89:11357–61. doi: 10.1073/pnas.89.23.11357.

39. Freeman WJ. Nonlinear gain mediating cortical stimulusresponse relations. Biol Cybern. 1979;13:237–47. doi: 10.1007/BF00337412.

40. Freeman WJ. Tutorial on neurobiology: from single neurons to brain chaos. Int J Bifurcation & Chaos. 1992;2:451–82. doi: 10.1142/S0218127492000653.

41. Dudkin AO, Sbitnev VI. Coupled map lattice simulation of epileptogenesis in hippocampal slices. Biol Cybern. 1998;78:479–86. doi: 10.1007/s004220050451.

42. Sbitnev VI. Bohmian trajectories and the path integral paradigm - complexified Lagrangian mechanics. In: Pahlavani MR, editor. Theoretical concepts of quantum mechanics. Rijeka: InTech; 2012. chapter 15, p. 313–34. doi: 10.5772/33064.

43. Zurek WH. Complexity, entropy, and the physics of information; Vol. 8, Boca Rato, London, New York: Taylor & Francis Group LLC; 1990. doi: 10.1201/9780429502880.

44. Taylor J. Lexical semantics. From Part III - aspects of linguistic analysis. In: Dancygier B, editor. Cambridge handbooks of cognitive linguistics. Cambridge: Cambridge University Press; 2017; chapter 16, p. 246–61. doi: 10.1017/9781316339732.017.

45. Meijer DKF, Jerman I, Melkikh AV, Sbitnev VI. Consciousness in the Universe is tuned by a musical master code. Part 1: a conformal mental attribute of reality. Quantum Biosyst. 2020;11:1–31.

46. Meijer DKF, Jerman I, Melkikh AV, Sbitnev VI. Consciousness in the Universe is tuned by a musical master code.Part 2: the hard problem in consciousness studies revisited. Quantum Biosyst. 2020;11:32–71.

47. Meijer DKF, Jerman I, Melkikh AV, Sbitnev VI. Biophysics of consciousness: a scale-invariant acoustic information code of a superfluid quantum space guides the mental attribute of the Universe. In: Bandyopadhyay A, Ray K, editors. Rhythmic oscillations in proteins to human cognition. Singapore: Springer Nature Singapore Pte Ltd.; 2021. chapter 8, p. 213–361. doi: 10.1007/978-981-15-7253-1.

48. Sbitnev VI. Hydrodynamical aspect of the physical vacuum. J Lasers Opt Photonics; International Conference on Quantum Mechanics and Applications, July 20-21, 2018 - Atlanta, Georgia, USA; 2018, Vol. 5. doi: 10.4172/2469-410X-C1-020.

49. Bohm D, Vigier JP. Model of the causal interpretation of quantum theory in terms of a fluid with irregular fluctuations. Phys Rev. 1954;96:208–16. doi: 10.1103/PhysRev.96.208.

50. Bohm D, Hiley BJ. An ontological basis for quantum theory: I. Non-relativistic particle systems. Phys Rep. 1987;144:322–48.

51. Bohm D. A new theory of the relationship of mind and matter J Am Soc Psychical Res. 1986;80:113–35. doi: 10.1080/09515089008573004.

52. Bohm D. Wholeness and the implicate order. London, New York: Taylor and Francis Group; 2006.

53. Landau L. On the theory of phase transition. Zh Eksp Teor Fiz. 1937;7:19-32.

54. López AG. Orbit quantization in a retarded harmonic oscillator. Chaos Solit Fractals. 2023;170:113412. doi: 10.1016/j.chaos.2023.113412.

55. Keener J, Sneyd J. Mathematical physiology. 2nd ed.; Vol. 8/I, Interdisciplinary Applied Mathematics, 8. New York: Springer Science+Business Media, LLC; 2009. doi: 10.1007/978-0-387-75847-3.

56. Mylvaganam S, Ramani M, Krawczyk M, Carlen PL. Roles of gap junctions, connexins, and pannexins in epilepsy. Front Physiol. 2014;5:172. doi: 10.3389/fphys.2014.00172.

57. Feuillet L, Dufour H, Pelletier J. Brain of a white-collar worker. The Lancet. 2007;370:262. doi: 10.1016/S0140-6736(07)61127-1.

58. Pollack GH. The fourth phase of water: beyond solid, liquid, and vapor. Vermont: University of Washington, Seattle; 2012.

59. Bell R. The proton in chemistry. 2nd ed. Golborne, Norwich: Chapman & Hall; 1973. Page 21: A theoretical analysis of proton mobility in water gave 2E-13 s, doi: 10.1007/978-1-4757-1592-7.

60. Sbitnev VI, Fedi M. Superfluid quantum space and evolution of the Universe. In: Capistrano de Souza AJ, editors. Trends in modern cosmology. Rijeka: InTech; 2017. chapter 5, p. 89–112. doi: 10.5772/68113.

61. Pollack GH. The fourth phase of water. Seattle (WA): Ebner and Sons Publ.; 2013.

62. Atkins P, de Paula J, Friedman R. Quanta, matter, and charge: a molecular approach to physical chemistry. New York; W. H. Freeman; 2009. Page 603, Table 18.5: Ionic mobilities in water at 298 K .

63. Brewer ML, Schmitt UW, Voth GA. The formation and dynamics of proton wires in channel environments. Biophys J. 2001;80:1691–702. doi: 10.1016/S0006-3495(01)76140-1.

64. Hassanali A, Giberti F, Cuny J, Kühne TD, Parrinell M. Proton transfer through the water gossamer. PNAS. 2013;110:13723–8. doi: 10.1073/pnas.1306642110.

65. Peng Y, Swanson JMJ, Kang SG, Zhou R, Voth GA. Hydrated excess protons can create their own water wires. J Phys Chem B. 2015;119:9212–8. doi: 10.1021/jp5095118.

66. DeCoursey TE. Voltage-gated proton channels and other proton transfer pathways. Physiol Rev. 2003;83:475–579. doi: 10.1152/physrev.00028.2002.

67. Potter KH. Indian metaphysics and epistemology. Delhi: Motilal Banarsidass; 1977

68. Beck F. Synaptic quantum tunnelling in brain activity. NeuroQuantology. 2008;6:140–51.

69. Feynman RP, Hibbs A. Quantum mechanics and path integrals. New York: McGraw Hill; 1965.

70. Sbitnev VI. Generalized path integral technique: nanoparticles incident on a slit grating, matter wave interference. In: Bracken P, editors. Advances in quantum mechanics. Rijeka: InTech; 2013. chapter 9, p. 183–211. doi: 10.5772/53471.

71. Sbitnev VI. Matter waves in the Talbot-Lau interferometry. J Phys Opt Sci. 2021;3:1–18. doi: 10.47363/JPSOS/2021(3)150.

72. Zampighi G. Gap junction structure. In de Mello WC, editors. Cell-to-cell communication. New York: Plenum Press; 1987. chapter 1, p. 1–28.

73. Meier C, Dermietzel R. Electrical synapses - gap junctions in the brain. In: Gundelfinger ED, Seidenbecher C, Schraven B, editors. Cell communication in nervous and immune system. Berlin, Heidelberg: Springer-Verlag; 2006. p. 99–128. doi: 10.1007/400_013.

74. The presentation. Chasti mozga. Available from: https://thepresentation.ru/biologiya/chasti-mozga. Accessed 16 Nov 2023. [In Russian].

75. Maxwell RW. Neurobiology of chakras and prayer. Zygon. 2009;44:807–24.

76. Connors BW, Long MA. Electrical synapses in the mammalian brain. Annu Rev Neurosci. 2004;27:393–418. doi: 10.1146/annurev.neuro.26.041002.131128.

77. Niculescu D, Lohmann C. Gap junctions in developing thalamic and neocortical neuronal networks. Cereb Cortex. 2014;24:3097–106. doi: 10.1093/cercor/bht175.

78. Volman V, Perc M, Bazhenov M. Gap junctions and epileptic seizures - two sides of the same coin? PLoS ONE. 2011;6:e20572. doi: 10.1371/journal.pone.0020572.

79. Penfield W. Mystery of the mind: a critical study of consciousness and the human brain. Princeton (NJ): Princeton University Press; 1975.

80. Vinogradova OS. The hippocampus and memory. Moscow: Nauka; 1975 [In Russian].

81. Kryukov VI. The role of the hippocampus in long-term memory: is it memory store orcomparator. J Integr Neurosci. 2008;7:117–84. doi: 10.1142/s021963520800171x.

82. Penfield W. The excitable cortex in conscious man (the Sherrington lectures). Liverpool: Liverpool University Press; 1958.

83. Penfield W, Jasper H. Epilepsy and the functional anatomy of the human brain. Boston (MA): Little Brown and Co.; 1954.

84. Eccles J, Feindel W. Wilder Graves Penfield, 26 January 1891–5 April 1976. Biogr Mem Fellows R Soc. 1978;24:473513. doi: 10.1098/rsbm.1978.0015.

85. Blom JD. A dictionary of hallucinations. New York: Springer Science + Business Media; 2010. doi: 10.1007/978-1-4419-1223-7.

86. Tong F. Out-of-body experiences: from Penfield to present. Trend Cognit Sci. 2003;7:104–6. doi: 10.1016/s1364-6613(03)00027-5.

87. Penfield W. Memory mechanisms. AMA Arch Neurol Psychiatry. 1952;67:178–98. doi: 10.1001/archneurpsyc.1952.02320140046005.

88. Saura CA, Parra-Damas A, Enriquez-Barreto L. Gene expression parallels synaptic excitability and plasticity changes in Alzheimer's disease. Front Cell Neurosci. 2015;9:318. doi: 10.3389/fncel.2015.00318.

89. Jirsa VK, Stacey WC, Quilichini PP, Ivanov AI, Bernard C. On the nature of seizure dynamics. Brain. 2014;137:221030. doi: 10.1093/brain/awu133.

90. Bragin A, et al. Analysis of chronic seizure onsets after intrahippocampal Kainic acid injection in freely moving rats. Epilepsia. 2005;46:1592-8.

91. Bragin A, et al. Analysis of Initial Slow Waves (ISWs) at the seizure onset in patients with drug resistant temporal lobe epilepsy. Epilepsia. 2007;48:1883–94.

92. Bragin A, Azizyan A, Almajano J, Engel Jr. J. The cause of the imbalance in the neuronal network leading to seizure activity can be predicted by the electrographic pattern of the seizure onset. J Neurosci. 2009;29:3660-71. doi: 10.1523/JNEUROSCI.5309-08.2009.

93. Borges FS, et al. Intermittency properties in a temporal lobe epilepsy model. Epilepsy Behav. 2023;39:109072. doi: 10.1016/j.yebeh.2022.109072.

94. Li L, Kriukova K, Engel Jr. J, Bragin A. Seizure development in the acute intrahippocampal epileptic focus. Sci Reports. 2018;8:1423. doi: 10.1038/s41598-018-19675-6.

95. Li L, Anatol Bragin A, Staba R, Engel Jr. J. Unit firing and oscillations at seizure onset in epileptic rodents. Neurobiol Dis. 2019;127:382-9. doi: 10.1016/j.nbd.2019.03.027.

96. Jin MM, Zhong C. Role of gap junctions in epilepsy. Neurosci Bull. 2011;27:389-406. doi: 10.1007/s12264-011-1944-1.

97. Gray JA. The neuropsychology of anxiety: an enquiry into the functions of the septo hippocampal system. New York: Oxford University Press; 1982.

98. Numan R. A prefrontal-hippocampal comparator for goaldirected behavior: the intentional self and episodic memory. Front Behav Neurosci Sec Learn Memory. 2015;9:323. doi: 10.3389/fnbeh.2015.00323.

99. Sbitnev VI, Chua LO. Local activity criteria for discretemap CNN. Int J Bifurcation Chaos. 2002;12:1227-72. doi: 10.1142/So218127402005157.

100. Charles A. Intercellular calcium waves in glia. Glia. 1998;24:39–49. doi: 10.1002/(sici)1098-1136(199809)24:1<39::aid-glia5>3.0.co;2-w.

101. Harris-White ME, Zanotti SA, Frautschy SA, Charles AC. Spiral intercellular calcium waves in Hippocampal slice cultures. J Neurophysiol. 1998;79:1045–52.

102. Huang *X*, et al. Spiral waves in disinhibited Mammalian neocortex. J Neurosci. 2004;24:9897–902. doi: 10.1523/JNEUROSCI.2705-04.2004.

103. Xu Y, Long X, Feng J, Gong P. Interacting spiral wave patterns underlie complex brain dynamics and are related to cognitive processing. Nature Human Behav. 2023;7:1196215. doi: 10.1038/s41562-023-01626-5.

104. Biktashev VN, Holden AV, Zhang H. Tension of organizing filaments of scroll waves. Philos Trans R S London, Ser

A: Math Phys Sci and Eng. 1994;347:611–30. doi: 10.1098/rsta.1994.0070.

105. Biktashev VN, Biktashevsa IV, Sarvazyan NA. Evolution of spiral and scroll waves of excitation in a mathematical model of ischaemic border zone. PLoS ONE. 2011;6:e24388. doi: 10.1371/journal.pone.0024388.

106. Chávez F, Kapral R, Rousseau G, Glass L. Scroll waves in spherical shell geometries. CHAOS. 2001;11:757–65. doi: 10.1063/1.1406537.

107. Cherry EM, Fenton FH. Visualization of spiral and scroll waves in simulated and experimental cardiac tissue. New J Phys. 2008;10:125016(43pp). doi: 1367-2630/10/12/125016.

108. Tang Q, et al. *In Vivo* mesoscopic voltage-sensitive dye imaging of brain activation. Sci Reports. 2016;6:25269. doi: 10.1038/srep25269.

109. Sbitnev VI. Checkerboard spiral waves in a 2D coupled map lattice. Int J Bifurcation Chaos. 1997;07:2569–75. doi: 10.1142/S0218127497001722.

110. Sbitnev V, Dudkin A. Checkerboard spiral waves in a 2D coupled map lattice. Scaling evidence. Int J Bifurcation & Chaos. 1999;9:919–28. doi: 10.1142/s0218127499000651.

111. Sbitnev V. 3D HH Scroll Waves O1 [Internet]. Available from: https://youtu.be/714ptgowO-k. Prepared 19 Aug 2023